Mechanical & Materials Engineering Faculty Publications

Mechanical & Materials Engineering, Department of

2020

Additive manufacturing of magnesium alloys

Rakeshkumar Karunakaran

Sam Ortgies

Ali Tamayol

Florin Bobaru

Michael P. Sealy

Additive manufacturing of magnesium alloys

Rakeshkumar Karunakaran, Sam Ortgies, Ali Tamayol, Florin Bobaru, Michael P. Sealy*

Department of Mechanical and Materials Engineering, University of Nebraska-Lincoln, 68588, USA

ABSTRACT

Magnesium alloys are a promising new class of degradable biomaterials that have a similar stiffness to bone, which minimizes the harmful effects of stress shielding. Use of biodegradable magnesium implants eliminates the need for a second surgery for repair or removal. There is a growing interest to capitalize on additive manufacturing's unique design capabilities to advance the frontiers of medicine. However, magnesium alloys are difficult to 3D print due to the high chemical reactivity that poses a combustion risk. Furthermore, the low vaporization temperature of magnesium and common biocompatible alloying elements further increases the difficulty to print fully dense structures that balance strength and corrosion requirements. The purpose of this study is to survey current techniques to 3D print magnesium constructs and provide guidance on best additive practices for these alloys.

1. Magnesium-based implants

Magnesium (Mg) alloys have emerged as a promising degradable biomaterial for use in orthopedics [1–9], cardiology [10–17], respirology [18,19], and urology [20]. The primary advantage of Mg is that long term complications can be minimized or avoided because the device completely degrades away. In orthopedics, another primary advantage is that Mg has a more comparable modulus to bone that minimizes the harmful effects of stress shielding.

To date, three companies have demonstrated clinical success and achieved regulatory approval in Europe and South Korea. In 2013, Syntellix received CE marking for a Magnezix® fracture compression screw that has sold more than 50,000 units [21]. In 2015, U&i Corporation received regulatory approval from the Ministry of Food and Drug Safety in South Korea for orthopedic bone screws made from a bioresorbable MgCa alloy referred to as Resomet [22]. U&i manufactures screws, K-wires, suture anchors, and pins with an Mg–Ca alloy that completely degrades in 6–18 months depending on the application. In cardiovascular health, Biotronik received CE marking for Magmaris in June 2016 and is the first clinically proven bioresorbable magnesium scaffold [23]. Although success has been demonstrated for smaller scale implants, such as screws and pins, current manufacturing technology is unable to provide bioresorbable constructs for more load-bearing applications that balance strength and corrosion requirements (Fig. 1).

Competing technologies that slow the corrosion rate of Mg-based biomaterials are coatings, alloying, and surface treatments (Fig. 2).

Coatings run the risk of uneven breakdown and cracking. They may only last a few weeks to a couple of months [24–26]. This may not be sufficient for such implants to safely pass the necessary threshold required by the recovery of bone's structural integrity (Fig. 3). Once the coating dissolves, uncontrolled corrosion of the alloy leads to excessive hydrogen gas build-up in the body and loss in strength of the implant.

Alloying can slow degradation an order of magnitude or more, which may still not be sufficient for many applications [27]. More importantly, the addition of rare earth metals has shown the most promise for improving the strength, but biocompatibility remains uncertain [27–29]. Alloying elements introduce a new toxicity risk. Controlled use of elements such as calcium, zinc, and manganese have shown to be non-toxic to the human body [3]. Alloyed implants were functional in the body for 6–8 weeks before degradation of the material resulted in a loss in strength. The hydrogen gas released in small quantities during the degradation of magnesium was considered harmless and could be removed using subcutaneous needles. At the microstructural level, these alloying elements affect grain size and distribution. The composition at the center of a grain is different from that at the grain boundary. The internal energy is higher at the grain boundary, and hence, corrosion takes place at these sites first. Another limitation of alloying is that regulatory approval is usually given for a fixed composition and thus a fixed corrosion rate. Any change to the alloy composition for a different patient population or application would require further regulator regulatory approval.

An alternative solution to adjust the corrosion rate is **surface**
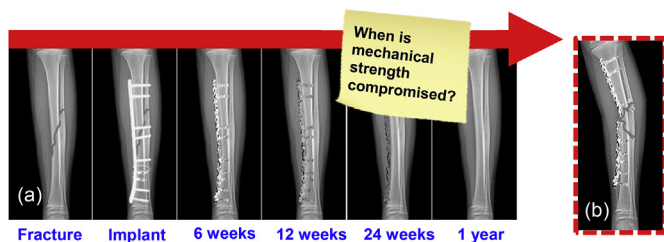

Fig. 1. Schematic representation of (a) normal degradation of a plate/screw construct in one year and (b) premature catastrophic failure due to stress shielding and stress-corrosion cracking.
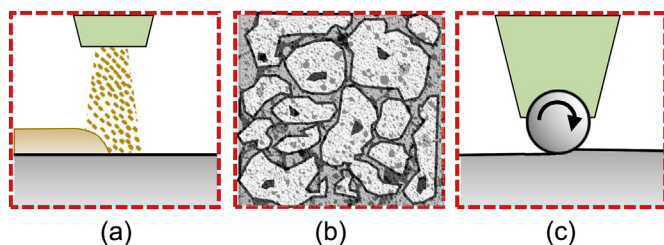

Fig. 2. Technologies to slow Mg corrosion: (a) coatings, (b) alloying, and (c) surface treatments.
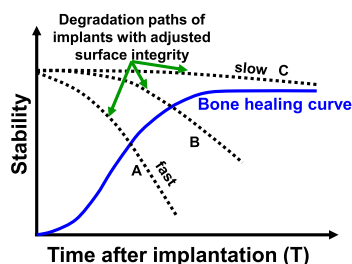

Fig. 3. Schematic diagram showing the intersection point between failure of medical implant relative to bone recovery.

treatments. Surface treatments offer clear advantages compared with the other approaches. Laser peening, for example, is a mechanical process where pressure waves caused by expanding plasma induces deep compressive residual stresses (CRS) and hardening up to 6 mm below the surface [30], which in turn, increases fatigue strength and corrosion resistance. Further, manipulating peening process parameters allows for tailoring degradation to patients' needs without biocompatibility concerns from changing composition or introducing a coating. Preliminary data has shown that mechanical surface treatments decrease Mg's corrosion rate [10,31–35]. The problem is that structural integrity is prematurely lost once the traditional surface treated layer degrades away [36].

2. Need for additive manufacturing of magnesium

Additive manufacturing (AM) of Mg alloys is of growing interest in the community due to enabling design capabilities not achievable with traditional manufacturing and its potential for development of biodegradable implants. Additive manufacturing of magnesium has been demonstrated using powder bed fusion [37–43], wire arc AM [44,45], paste extrusion deposition [46], friction stir AM [47], and jetting technologies [48,49]. These processes have different process mechanics and forms of raw materials. Each process yields AM components having different structural properties. By manufacturing components in this way, AM can be used to develop highly complex geometries that are either difficult or impossible to make using conventional machining processes. AM enables individualized implants that more closely align with anatomical geometries. Also, AM reduces the manufacturing time and cost for implants as multiple steps of conventional machining may be eliminated and batch processing becomes feasible.

The ability to produce complex internal and external geometries using AM enables the development of geometrical features that promote cell growth, proliferation, and bone regeneration. Scaffolds of WE43, a magnesium alloy with yttrium and rare earth metals, printed with pores as small as 600 μm demonstrated less than 25% toxicity *in vitro* and maintained structural rigidity for four weeks (Fig. 4 and Fig. 5) [50]. Furthermore, porous depositions are attainable using AM, which may act as favorable sites for tissue adhesion that accelerate the healing process. Porosity is adjustable across a 3D construct by manipulating print process parameters, which will directly affect corrosion rates and cell behavior.

The existing polymer based biodegradable implants lack the required strength to be used as load bearing orthopedic implants. The similar stiffness between human bone and magnesium avoids stress shielding and makes and ideal candidate for such load bearing implants. Furthermore, a comparison of magnesium alloys with polylactide polymer, which is an existing biodegradable polymer used for non-load bearing implants showed higher bone cell generation in magnesium implants (Fig. 6) [2,51]. This experiment used magnesium and polylactide femoral implant rods *in vivo* in guinea pigs.

3. Challenges with additive manufacturing of magnesium

In recent years, AM of reactive materials, particularly magnesium, has been of interest in the research community and technology is being developed to minimize the difficulties associated with 3D printing. Magnesium is a difficult metal to 3D print due to its highly reactive nature. Magnesium oxidizes uncontrollably in its pure form and must be stored in a manner that prevents exposure to oxygen. Raw materials for AM are available in powder, liquid resin, or wire forms. In this state, the surface energy of the metal increases and poses a higher risk of reacting with atmospheric oxygen to enable combustion. These risks have resulted in inadequate research into manufacturing processes for magnesium to be used as a potential biodegradable alloy. Specialized
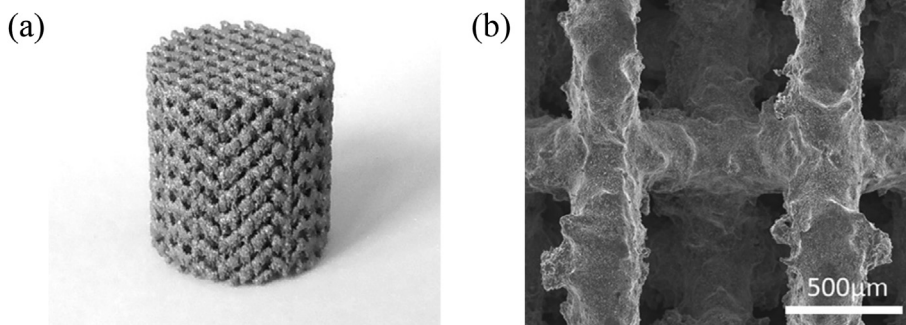

Fig. 4. (a) As-printed WE43 scaffold and (b) surface morphology of as-polished strut [50].
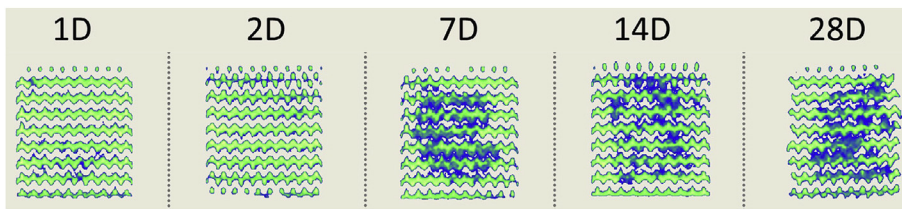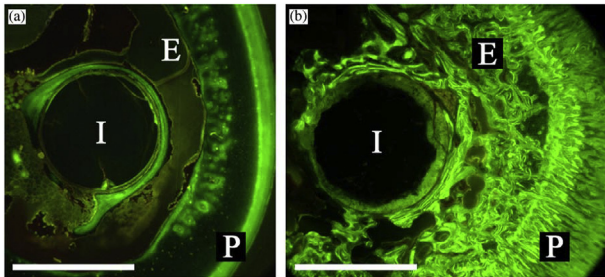
Fig. 6. Flouroscopic images of cross-sections of a (a) degradable polymer and (b) and a magnesium rod with *in vivo* staining of newly formed bone [2,51].

equipment that is capable of printing magnesium in inert atmosphere is required, while also ensuring safe means of material handling.

4. Powder bed fusion of magnesium alloys

Powder bed fusion (PBF) is an AM process in which thermal energy is used to selectively fuse regions of a powder bed [52]. The powder bed contains metal, polymer, or ceramic powder as feedstock. An energy source directed towards the powder bed selectively scans and melts the top layer of the powder bed. The powder bed then lowers and a fresh layer of powder is spread over the melted layer (Fig. 7). This process continues until the entire structure has been formed by stacking melted layers of powder. The powder used in PBF varies between 20 μm and 150 μm but it usually tends to be on the lower end of this range.

PBF has a wide variety of parameters that can cause variations in the chemical composition, mechanical properties, and geometry of manufactured components. Accounting for all the parameters will be tedious. Therefore, it is important to identify and focus on the important parameters, such as laser power, scanning speed, and layer thickness. One way to determine the significant parameters in magnesium PBF is by design of experiments (DOE) [40]. DOE is a statistical method that helps reduce the cost and time taken to find the significant parameters by reducing the number of experiments. A magnesium

Fig. 7. Schematic diagram of a PBF System [53].

alloy, AZ31, consisting aluminum, zinc, and manganese was printed on a PBF system [45]. The parameters influencing PBF of AZ31 were analyzed using DOE, and it was seen that high laser power reduces porosity drastically. It also shows that a reduction in laser scanning speed at constant laser powder yielded porous parts. Hence, laser power and scanning speed need to be carefully considered during PBF of Mg. The parameters that affect PBF of Mg are described below.

4.1. Laser power and scanning speed

Lasers are the most widely investigated energy source for PBF of magnesium alloys. Lasers cause a high concentration of heat to be focused over small regions of the powder bed for limited amounts of time to melt the powder. This short-timed heat flux causes rapid heating and quenching of the molten powder leading to rapid solidification. This rapid solidification results in grain refinement, which enables the material to withstand larger loads.

When magnesium alloy powder is subjected to high temperatures, some elements in the powder undergo vaporization [39]. Powder vaporization leads to a localized buildup of vapor pressure at the melt pool during material deposition. The pressure causes molten material in the melt pool to spatter outward, which leads to the formation of a low-density structure. This also results in variations in chemical composition as compared to the original powder. Good solubility of the alloying elements during AM is important for minimizing the formation of galvanic cells in printed components that would interfere with corrosion behavior [54].

Laser power and scanning speed significantly influence the melt pool, vaporization, and resulting deposition in PBF. Although the effects of varying laser power and scanning speeds individually cause alterations in the quality of depositions, it is difficult to describe their effects individually. Together, they play a major role in determining the energy density of the laser being transferred to the magnesium powder [41,55]. Energy density (E_v) is given by equation (1):

$$E_v = \frac{P}{S*T*V} \tag{1}$$

where *P*, *S*, *T*, and *V* represent laser power, hatch spacing, layer thickness, and scanning velocity, respectively. From this equation, it is seen that the same energy density can be attained for different values of laser powers and scanning speeds.

The majority of literature on printing magnesium pertains to alloys; however, pure magnesium powder having spherical particles with a mean size of 24 μm used at a relatively low energy density of 155.56 J/mm³ yielded 97.5% dense depositions [56]. The relative density and mechanical strength of the material reduced when the energy density was increased or decreased.

ZK60 is a magnesium alloy with zinc and zirconium. When ZK60 powder was subjected to very high energy density of 1250 J/mm³, magnesium and zinc elements within the powder underwent heavy vaporization [39]. When the laser density was decreased to 250 J/mm³, the melt pool stabilized and reduced the vapor pressure. As a result, incomplete fusion of powder particles lead to a poor relative density of 82.25% (Fig. 8). A maximum relative density of 94.05% was achieved at an energy density of 416.67 J/mm³.

WE43 is a magnesium alloy containing yttrium and neodymium as the main alloying elements. A relative density of 99.4% was achieved
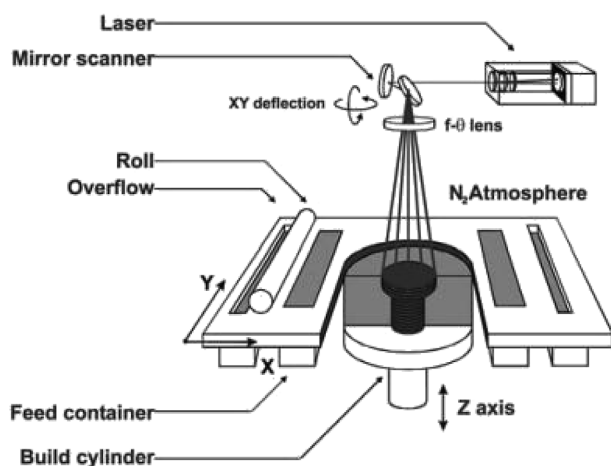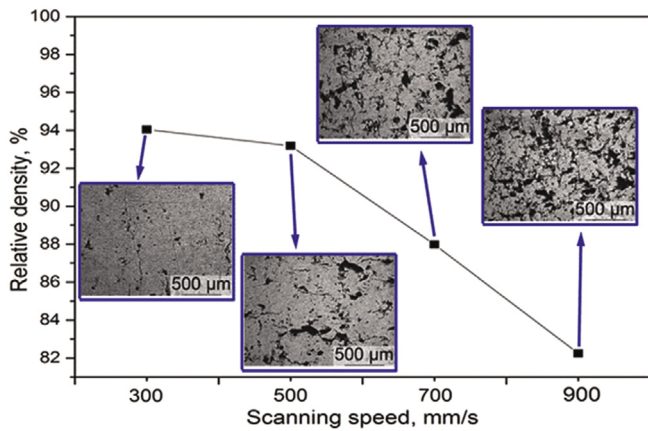
Fig. 8. Influence of laser scanning speed on relative density of ZK60 [39].

Fig. 10. Grain size variation of Mg–9%Al powder as a function of laser power and scan speed [59].

by printing WE43 at an energy density of 238 J/mm^3 [54]. This suggests that optimal print parameters for magnesium alloys tend to exist at low energy densities at which the resultant part density is high and vaporization of the alloying elements at the melt pool is low. There also exist a minimum energy density level at which porosity increases. An energy density of 18.8 J/mm^3 achieved by decreasing the laser power (195 W–135W) while simultaneously increasing the scanning speed (800 mm/s to 1200 mm/s) resulted in the porosity increasing from 0.4% to 17% (Fig. 9) [57]. The dynamic strength measured by split Hopkinson pressure bar testing decreased with lower energy densities. WE43 alloy could also be used to build porous scaffolds composed of diamond unit cells. It was possible to achieve a strut size of 400 μm in the unit cells at a low energy density of 100 J/mm^3 [58].

Mg–9%Al alloy was completely melted at a 15 W laser power and scanning speed of 20 mm/s (Fig. 10) [59]. This corresponds to a laser energy density of 187.5 J/mm^3. Another study on the same material found good depositions at an energy density of 155.6 J/mm^3, which indicates Mg–9%Al alloy may have a range of acceptable energy density regions [38]. It is important to note that this range of energy density is influenced by several parameters including powder quality and layer thickness.

It was also observed that the optimal process parameters are different for obtaining dense structures as compared to obtaining structures having good surface quality (Fig. 11) [60]. A Mg–Al–Zn alloy (AZ61) with mean particle size of 48 μm was seen to obtain good surface quality at energy densities of 179–250 J/mm^3. The alloy required lower energy density of 156 J/mm^3 to develop structures having 99.4% relative density. The mechanical properties also improved at this lower energy density for AZ61 alloy. Hence, a possible method to obtain highly dense depositions with good surface quality is to use different process parameters for the interior and surface of the depositions.
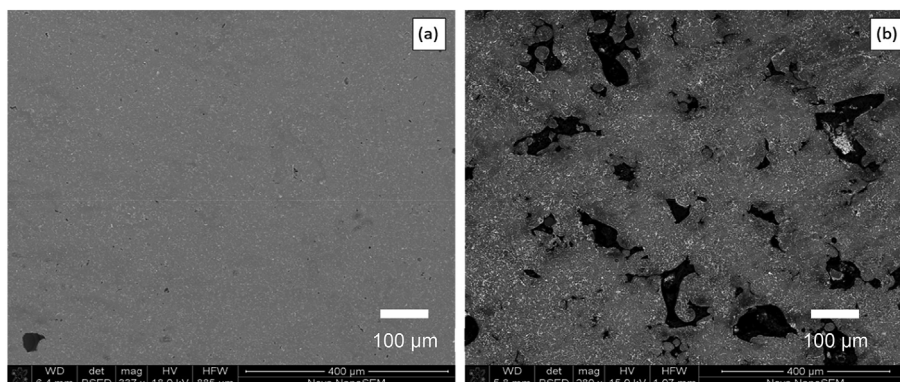
Optimal print parameters for another Mg–Al–Zn alloy AZ91D were seen to be around 200 W and 0.09 m/min scanning speed [61]. The corresponding energy density ranged from 83 J/mm^3 to 167 J/mm^3. This result is complimented by another study on AZ91D which saw the smoothest depositions at an energy density of 122 J/mm^3, which shows that a lower energy density is required for the AZ91D as compared to Mg–9%Al [62].

Use of bioactive glass along with PBF printing of Mg–Zn–Zr alloy (ZK30) has also been shown to improve corrosion resistance through *in vitro* studies [63]. Bioactive glass promotes deposition of Ca–P compounds, which are highly compatible and similar to bone minerals. Interestingly, these depositions were performed at a very high energy density of 1875 J/mm^3. Corrosion resistance of the ZK30 magnesium alloy in simulated body fluid was found to increase with rising quantities of bioactive glass in the ZK30 powder mixture. Addition of 10 wt % bioactive glass increased corrosion resistance and cytocompatibility of the deposited alloy.

4.2. Layer thickness

The thickness of layers dictates the speed of the printing. Smaller layer thickness results in a higher number of times the powder is spread over the powder bed. A thick layer of powder spread over the powder bed may result in insufficient melting. It was seen that the smoothness of depositions for pure Mg powder existed only until the layer thickness reached 0.25 mm [42]. Above 0.25 mm, the surface contained pores (Fig. 12). With higher layer thickness, the amount of material in the
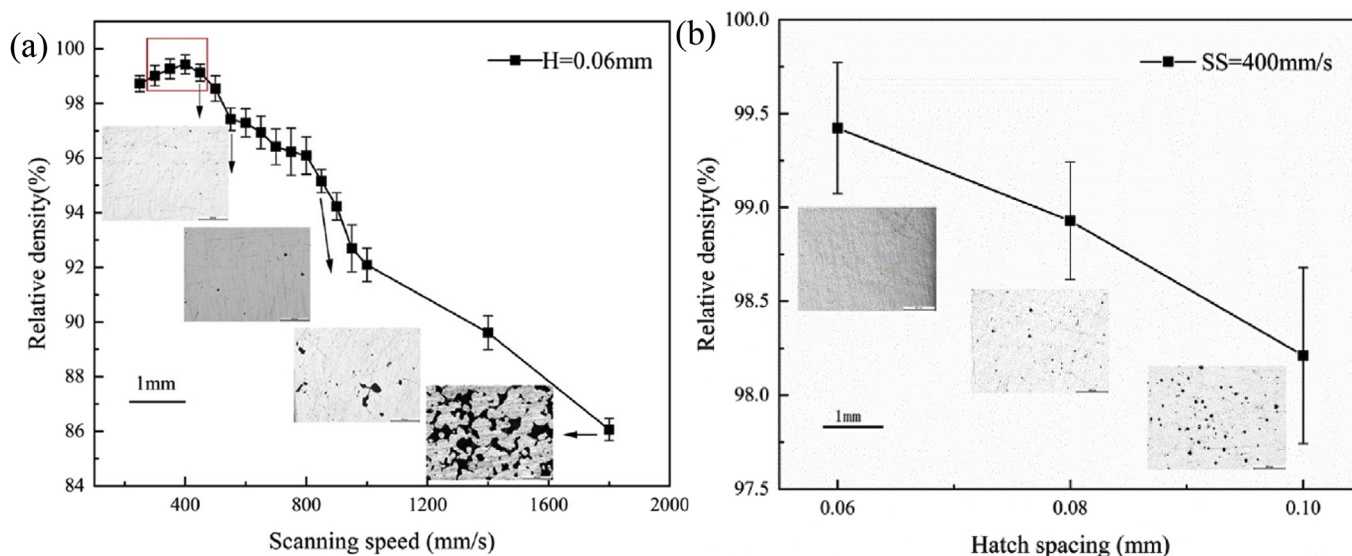

Fig. 9. Porosity of structures fabricated at (a) 40.6 J/mm^3 produces dense structure and (b) 18.8 J/mm^3 produces porous structure [57].

Fig. 11. Relative density obtained by PBF of AZ60 alloy [60].

melt pool also increased. The powder then was seen to require higher laser energy density to melt. Insufficient energy density leads to inadequate melting of powder particles and porosity in the depositions.

For AZ91, optimal layer thickness was in the range of 25–45 μm [62]. Layers thicker than 50 μm saw a sudden increase in defects and a fall in hardness. Interestingly, it was observed that varying layer thickness did not influence the AM process as much as parameters like hatch spacing and laser power.

4.3. Magnesium powder

The surface energy of the magnesium powder is high due to the small particle size. As a result, Mg powder readily oxidizes and becomes difficult to deposit in layers. Hence, alloying is generally used to reduce oxidation sensitivity. Some of the common non-toxic alloying elements include calcium, zinc, and manganese. These elements affect the obtained grain structure, strength, and heat resistance of magnesium [64].

The quality of depositions is dependent on the powder particle size (Fig. 13) [65]. Larger Mg powder particles with mean particle size of 43 μm achieved 96.13% relative density while smaller Mg powder having mean size of 26 μm yielded depositions with 95.28% relative density. Printing smaller powder particles raised the melt pool temperature and resulted in aggressive oxidation. Even bigger powder particles of 75–150 μm failed to form molten or sintered depositions [55].

Alloying elements in magnesium used in PBF also affect the quality of depositions (Fig. 14) [66]. A lower presence of aluminum in AZ61 magnesium alloy powder resulted in loss of relative density in the depositions, while Zn content higher than 1 wt% resulted in solidification cracks and micro-cracks in the depositions.

4.4. Build envelope conditions

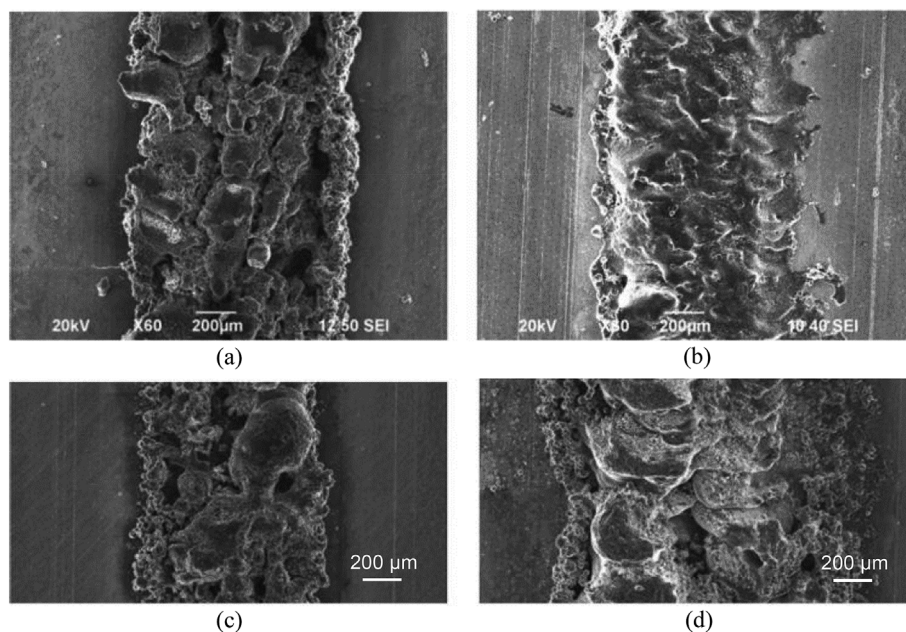Chamber Pressure: Magnesium is a difficult material to use in

Fig. 12. Surface of deposited pure magnesium for thickness of (a) 0.25 mm non-preheat, (b) 0.25 mm preheat, (c) 0.30 mm non-preheat, and (d) 0.30 mm preheat [42].
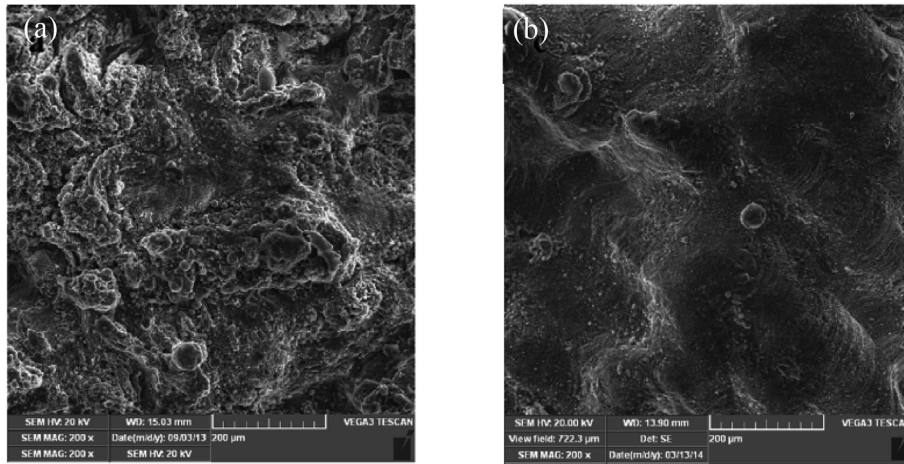
Fig. 13. Surface morphology for PBF deposition of pure magnesium with (a) 26 μm and (b) 43 μm powder particle sizes [65].
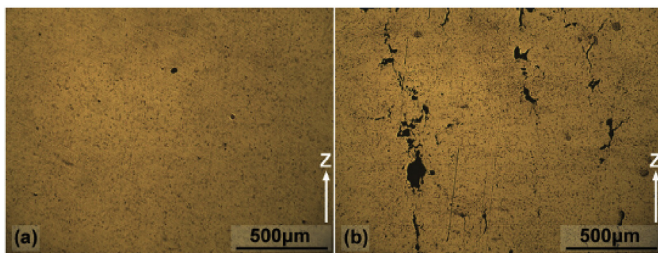

Fig. 14. Defects in PBF of (a) Mg–1Zn and (b) Mg–2Zn. Modified from Ref. [66].
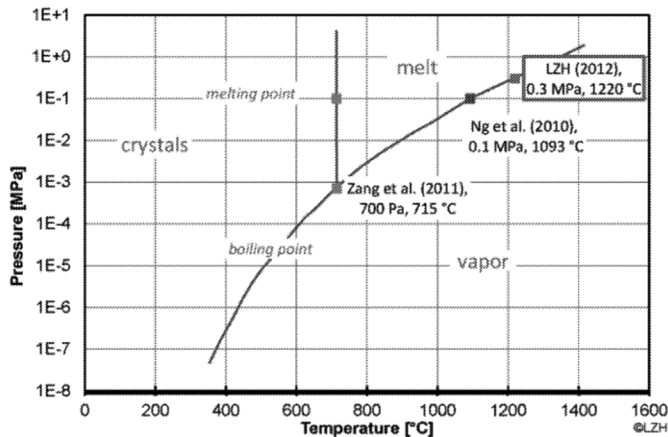

Fig. 15. Magnesium phase diagram [37].

Fig. 16. Mass gain due to oxidation of Mg powder for different rates of heating [67].

additive manufacturing due to its relatively low boiling point (1,093 °C) in relation to its melting point (650 °C), and it has a low evaporation heat of 5.272 kJ/kg when at ambient temperature [37]. The consequence is powder evaporates instead of melting. One proposed solution was to over-pressurize the build chamber to raise the melting temperature (Fig. 15). The melting temperature of magnesium increased to 1220 °C by pressurizing the build chamber to 300 kPa. The temperature of laser during printing can be increased due to increase in melting temperature of Mg. Higher operation temperature also reduces the dynamic viscosity of molten depositions, which affects layer thickness and hatch spacing. It is important to note that an exothermic reaction of magnesium powder with residual amounts of oxygen in the pressurized build chamber can lead to an explosion, and therefore, is a safety hazard.

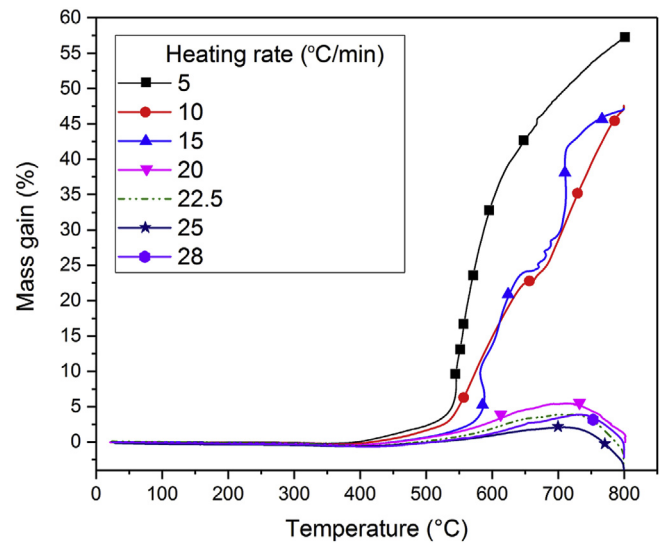Oxygen level: Magnesium has a high affinity for oxygen in atmosphere to form magnesium oxide. Even under an inert atmosphere, such as highly purified argon, small amounts of oxygen are present. At temperatures above 400 °C, magnesium reacts with residual amounts of oxygen to form magnesium oxide (Fig. 16) [67]. During PBF, the oxide layer breaks down and settles at the grain boundaries. This creates voids in the depositions, which leads to micro cracks. One way to reduce the oxidation is to increase the layer thickness. By this approach, oxidation is reduced within layers and is concentrated at the layer interfaces. Another way powder oxidation occurs is due to recycling of powder. As the powder in the powder bed undergoes multiple heating cycles, the proximity to the moving heat flux due to the laser can cause powder oxidation due to exposure to high temperatures.

Preheating: Preheating the build platform affects build quality significantly in PBF [42]. Preheating lowers the heat flux between the heat source and powder causing depositions to be smoother and flatter (Fig. 17). Preheating also improved the wettability and surface roughness of 3D printed magnesium (Fig. 18).

5. Wire arc additive manufacturing of magnesium

An alternative method for additive manufacturing is wire arc additive manufacturing (WAAM), which is a type of Directed Energy Deposition (DED) AM. DED systems use focused thermal energy to fuse
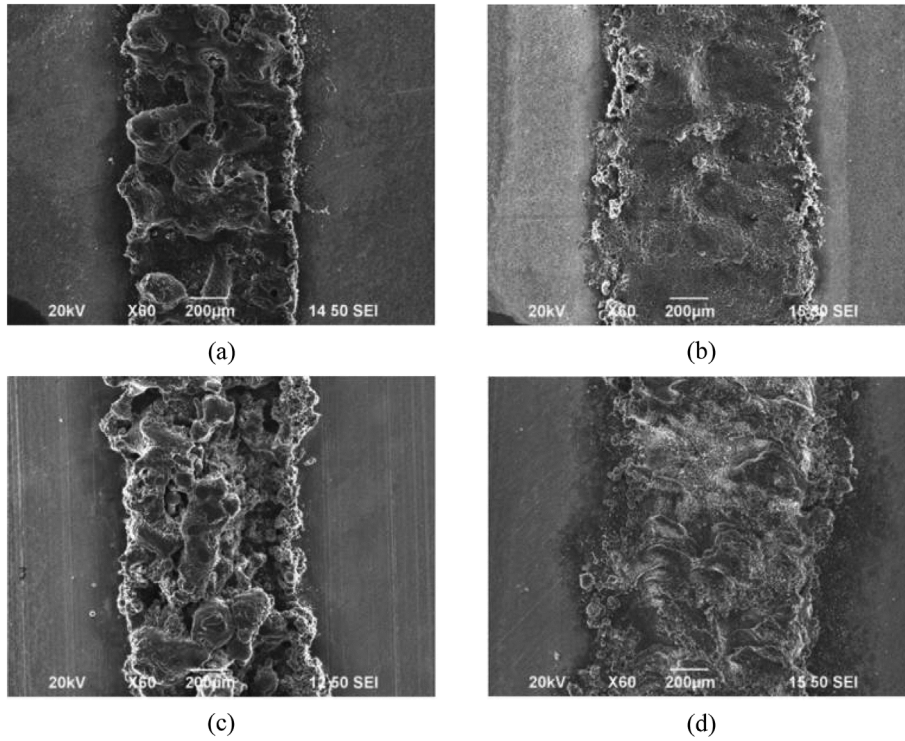
(a)   (b)

(c)   (d)

Fig. 17. Surface of deposited magnesium for layer thickness of (a) 0.15 mm non-preheat, (b) 0.15 mm preheat, (c) 0.20 mm non-preheat, (d) 0.20 mm preheat [42].
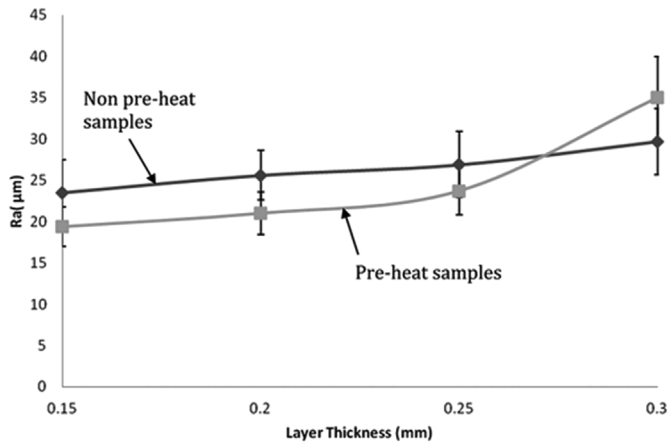

Fig. 18. Effect of preheating on roughness of deposition [42].
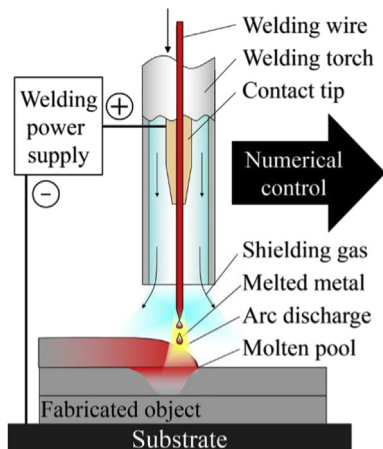

Fig. 19. Material deposition for wire arc additive manufacturing [68].

materials by melting as they are being deposited [52]. WAAM based DED systems (Fig. 19), have a metal wire that is fed at a constant rate and melted by an arc onto the previously deposited layers. WAAM is based on the two wire-based welding methodologies: tungsten inert gas (TIG) and metal inert gas (MIG). Compared to other DED processes, WAAM has the advantages of having a higher deposition rate, efficiency in material usage, and a lower cost [68].

For MIG-based WAAM of AZ31B, speed and feed affect the microstructure of the sample [68]. Smaller grains were observed as the speed and feed during the process was increased (Fig. 20). Also, WAAM was found to produce higher density components compared to PBF. The tensile strength of WAAM manufactured components were comparable to rolled AZ31B. WAAM of magnesium alloy AZ80 M showed a microstructure similar to as-cast quenched AZ80 M alloy [44].

For TIG WAAM of AZ31 magnesium alloy, it was found that the quality of depositions heavily depended on the arcing frequency during the deposition process [45]. As shown in Fig. 21, ripples during deposition become finer as the frequency of arcing is increased. With higher pulse frequency, the surface tended to become smoother.

It was also observed that in all the depositions, fully dense parts were obtained. The grain size of the alloy in the depositions also changed significantly due to the variation in arc pulse as indicated in
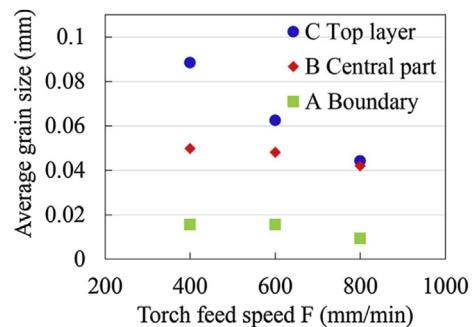

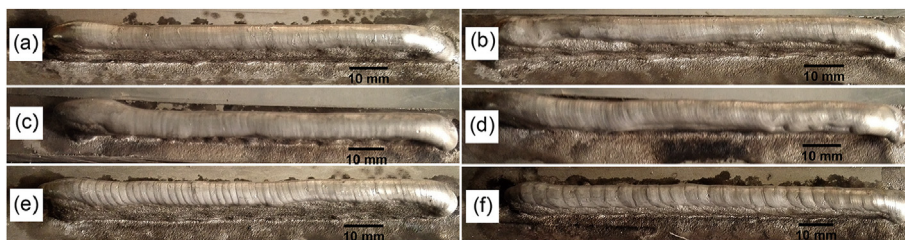**Fig. 20.** Optical micrograph of fabricated material [68].

Fig. 21. WAAM depositions of AZ31 at (a) 500 Hz, (b) 100 Hz, (c) 10 Hz, (d) 5 Hz, (e) 2 Hz, and (f) 1 Hz [45].

Fig. 22. Smallest grains were observed at frequencies of 5–10 Hz. Coarser grains were seen when deposition took place at frequencies higher or lower than this frequency. Also, the tensile strength was found to be the highest at this frequency.

6. Paste extrusion deposition

The previously discussed techniques of AM were based on melting and deposition of material. While the powder melting based processes resulted in structurally strong parts, in some cases they may turn out to be detrimental to production of high functioning magnesium implants. For the implant to be readily accepted by the body and to fasten the healing process, the implant material needs to resemble the bone tissue composed of hydroxyapatite and collagen type I [46]. These are ceramic-based inorganic and organic composites, respectively. The organic portion of the material cannot withstand the high temperatures typically seen in the AM processes such as PBF.

Powder extrusion deposition is a process in which a paste is extruded from a syringe over a base plate (Fig. 23). The base plate is moved relative to the syringe to form the desired 3D contours. Once the deposition is completed, the paste is dried to harden the deposited material from the syringe. It should be noted that this process does not involve high temperature heating. When pure magnesium mixed with different percentages of gelatin for manufacturing scaffolds, it was found that gelatin adds strength to the scaffolds. However, the overall strength was still found to be much lower compared to other fusion-based AM process. It is important to note that this process is still valuable for prospective magnesium implants as the paste used to manufacture components can also contain drugs that can help quicken the healing process of the body.

7. Friction Stir Additive Manufacturing of magnesium

Friction Stir AM (FSAM) is a type of sheet lamination process in which sheets of material are bonded together to form a part [52]. FSAM
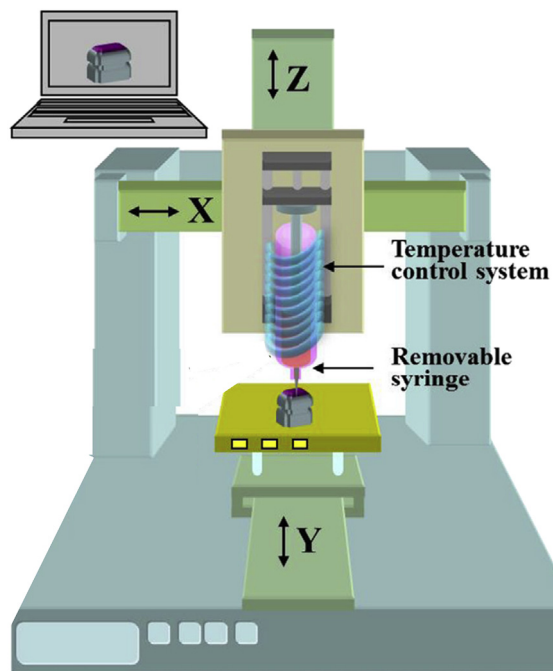
Fig. 23. Set-up for paste extrusion deposition [46].

uses heat due to friction between rotating tool and layer to be bonded to plastically deform and fuse layers of material together (Fig. 24). This process imparts high strength and ductility to components. Components manufactured from FSAM of WE43 Mg alloy exhibited very high strengths and a tenfold increase in ductility as compared to stock WE43; however, porosity remained a major issue [47]. As the heat due to friction increased at higher tool rotational speeds, more material was forced outward from the tool. Also, high amounts of residual stress were
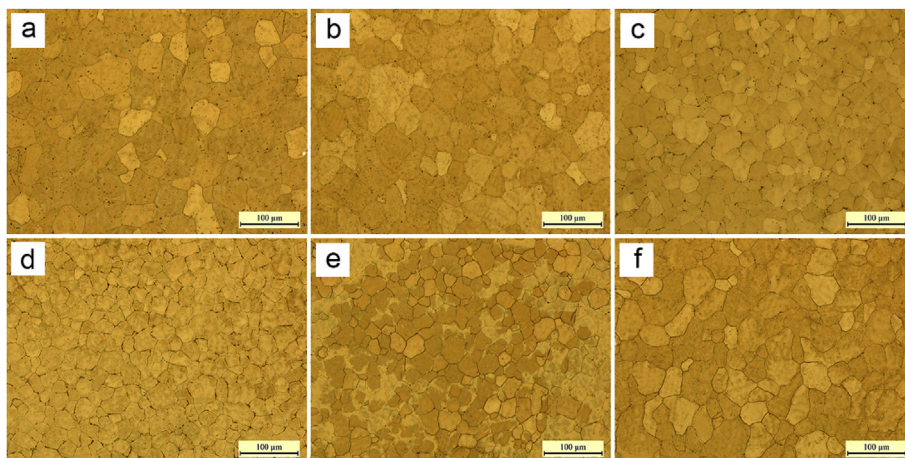
Fig. 22. Microstructure of depositions at frequencies of (a) 500 Hz, (b) 100 Hz, (c) 10 Hz, (d) 5 Hz, (e) 2 Hz, and (f) 1 Hz [45].
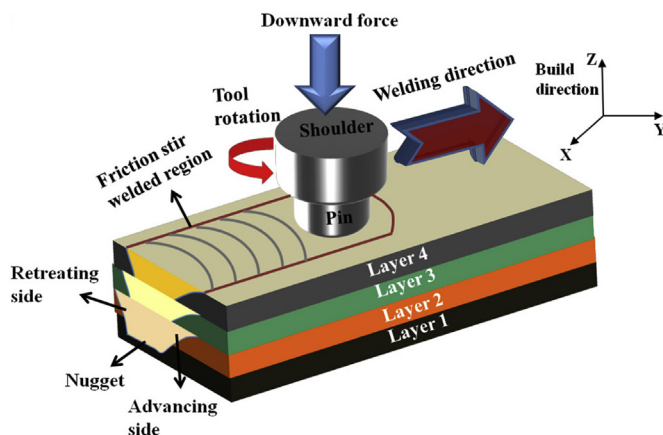
Fig. 24. Schematic of friction stir welding [47].

imparted into the material due to high thermal gradients in the weld cross-section.

8. Jetting technologies for magnesium

8.1. Binder jetting

Binder jetting is an AM process in which droplets of liquid binding agent are selectively deposited to join particles spread over a powder bed [52]. One advantage of binder jetting is the ability to fabricate structures at room temperature [69]. Incorporating organic, biologically active, or hydrated molecules within the bulk is possible. Printing is accomplished by spreading a layer of powder on the build plate followed by deposition of a binding agent that hardens and binds particles together. The process is repeated layer by layer until the desired geometry is obtained. Binder jetting has an ideal particle size in the range of 15–35 μm and has an approximate resolution of 20–30 μm. Biodegradable magnesium phosphate (MgP) scaffolds were successfully manufactured using binder jetting [70,71]. The tensile and compressive strength of these scaffolds were comparable to the human bone.

8.2. Binder-less jetting

Binder-less jetting is a process in which capillary forces within the powder act as the binding agent to adhere powder particles (Fig. 25) [48]. A single phase solvent was used to adhere layers of pure Mg powder. The deposited material was baked at 650 °C to sinter and harden the printed part and exhibited no solvent contamination. Binder-less jetting was used to print a Mg–Zn–Zr alloy with porosity of 29% and average pore size of 15 μm [49]. The material strength was directly proportional to the holding time during sintering. It was possible to achieve a compressive strength of 174 MPa and a modulus of 18 GPa using binder-less jetting, which is comparable to human bones.

9. Biocompatibility and antibacterial properties of 3D printed magnesium alloys

Magnesium has been shown to be biocompatible for the human body in several studies [51,72,73]. The human body requires an intake of about 350–400 mg of magnesium every day. Hence, the dissolution of Mg^{2+} ions in the human body during the implant degradation is not expected to cause any bodily damage. No risks of magnesium overdose have been cited in literature. The only cited issue with *in vivo* use of magnesium is the excess hydrogen formation due to corrosion reaction within the human body [74].

Incorporating antibacterial characteristics into implants is important to prevent infections inside the human body. Magnesium does not exhibit any antibacterial properties as seen in *in vitro* studies [75]. Bacterial activity reduced when traditionally manufactured and 3D printed magnesium alloys were coupled with copper. However, traditional manufacturing methods have not been able to deliver good quality Mg–Cu components due to issues of galvanic corrosion. AM has been able to overcome this challenge for small amounts of copper in the magnesium alloy below the solid solubility limit [75,76]. The mixing of 0.4 %wt copper powder with ZK60 was found to reduce *Escherichia Coli* colony count to zero after 72 h under normal pH conditions.

Use of bioactive glass along with magnesium alloys has also been shown to improve cytocompatibility [63]. Further, degradation resistance of the ZK30 magnesium alloy in simulated body fluid was found to increase with rising quantities of bioactive glass in the ZK30 powder mixture in PBF that would limit Mg ion release within the body.

10. Summary and conclusions

This work summarizes additive manufacturing technologies used to print magnesium. Reactivity of magnesium makes it a difficult material to print biodegradable implants due the high surface energy of the powder and high electronegativity of the alloy that drives the rapid corrosion rate within the human body. However, these challenges are being overcome steadily by multiple approaches in AM. The attempts at printing Mg using PBF, WAAM, paste extrusion deposition, FSAM, and jetting technologies have been described with focus on their process parameters. Powder bed fusion is the most widely investigated method for printing magnesium alloys due to the relatively small heat flux and complex internal and external geometries enabled by this technology. Depending upon the type of magnesium alloy used, parts with a density of 96.13% have been achieved. Creating near fully dense structures above 99% remains a critical challenge in magnesium AM. Despite relatively high levels of porosity, the manufactured parts have demonstrated the ability to retain stiffness up to four weeks *in vitro*. The various factors that influence the AM processes discussed in this review are summarized below:

Powder Bed Fusion

Laser Power and Scanning Speed	A wide range of laser power and scanning speeds can be deemed as optimal; however, a low laser energy density between 50 and 200 J/mm^3 is critical. High energy density leads to element vaporization while low energy density leads to insufficient melting of Mg powder. Energy density is dependent of alloy composition.
Layer Thickness	Layer thickness above 250 μm for pure Mg prevented complete fusion and resulted in higher porosity
Powder Size	Magnesium powder of 50 μm for pure Mg was seen to yield better depositions compared to smaller or larger powders. Particles that are too small result in higher rates of vaporization and particles that are too big do not achieve a full melt
Build Envelop Conditions	The vaporization temperature of magnesium increases with higher chamber pressures. This facilitates higher operation temperatures for printing Mg. However, safety risks increase by this approach. Also, preheating of the work table before printing leads to smoother depositions.

Wire Arc Additive Manufacturing

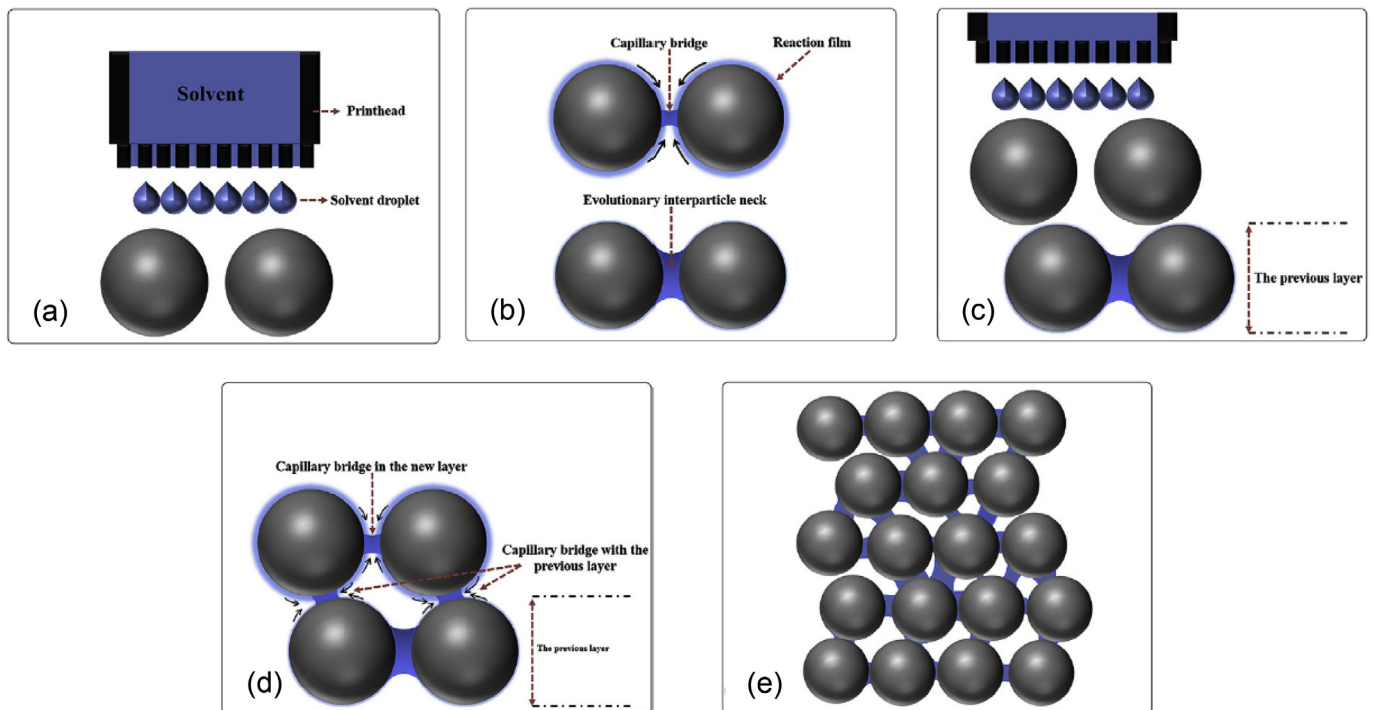|	
Deposition Speed and Feed	Higher speeds and feeds of deposition resulted in more refined, smaller grains.
Arc Frequency	Small refined grains were observed at arcing frequency of 5–10 Hz for TIG WAAM. Grain size was found to increase above and below this frequency range.

Fig. 25. Principle of binder-less jetting: a) solvent deposition, b) Development of capillary bridges among wet particles, c) spreading of next powder layer, d) capillary action forms bridges between particles in new and previous layers, and e) fully developed solid structure is formed after drying and sintering [48].

Paste Extrusion Deposition

Extrusion Temperature	Flowability of paste was found to increase at higher temperature during extrusion.
Paste Composition	Higher quantities of gelatin in MgP-gelatin mixture resulted in stronger manufactured samples. However, the strength was still much lesser than other sintering or fusion based AM processes.

Friction Stir Additive Manufacturing

Tool Rotational Speed	Higher tool force and speeds resulted in higher cladding temperatures, which led to higher porosity in the components.
Tool Force	Higher tool force increases temperature due to friction, and thus, residual stresses in components increases.

Jetting Technologies for Additive Manufacturing

Binder Jetting	100% recyclability of powder. Binding agent must be chosen carefully by considering its reactivity with powder.
Binder-less Jetting	Prevents contamination due to absence of binding agent.

Magnesium is a promising material for the biomedical industry due to its biodegradability and biocompatibility. AM of magnesium enables more intricate geometries and new design for manufacturing paradigms linked to implant performance.

Declaration of competing interest

The authors declare that they have no known competing financial interests or personal relationships that could have appeared to influence the work reported in this paper.

References

[1] Y. Chen, Z. Xu, C. Smith, J. Sankar, Recent advances on the development of magnesium alloys for biodegradable implants, Acta Biomater. 10 (2014) 4561–4573.

[2] M.P. Staiger, A.M. Pietak, J. Huadmai, G. Dias, Magnesium and its alloys as orthopedic biomaterials: a review, Biomaterials 27 (2006) 1728–1734.

[3] F. Witte, N. Hort, C. Vogt, S. Cohen, K.U. Kainer, R. Willumeit, F. Feyerabend, Degradable biomaterials based on magnesium corrosion, Curr. Opin. Solid State Mater. Sci. 12 (2008) 63–72.

[4] Y. Xin, T. Hu, P.K. Chu, In vitro studies of biomedical magnesium alloys in a simulated physiological environment: a review, Acta Biomater. 7 (2011) 1452–1459.

[5] N. Erdmann, A. Bondarenko, M. Hewicker-Trautwein, N. Angrisani, J. Reifenrath, A. Lucas, A. Meyer-Lindenberg, Evaluation of the soft tissue biocompatibility of MgCa0.8 and surgical steel 316L in vivo: a comparative study in rabbits, Biomed. Eng. Online 9 (2010) 63.

[6] C. Castellani, R.A. Lindtner, P. Hausbrandt, E. Tschegg, S.E. Stanzl-Tschegg, G. Zanoni, S. Beck, A. Weinberg, Bone–implant interface strength and osseointegration: biodegradable magnesium alloy versus standard titanium control, Acta Biomater. 7 (2011) 432–440.

[7] S.E. Henderson, K. Verdelis, S. Maiti, S. Pal, W.L. Chung, D. Chou, P.N. Kumta, A.J. Almarza, Magnesium alloys as a biomaterial for degradable craniofacial screws, Acta Biomater. 10 (2014) 2323–2332.

[8] H. Waizy, J. Diekmann, A. Weizbauer, J. Reifenrath, I. Bartsch, V. Neubert, R. Schavan, H. Windhagen, In vivo study of a biodegradable orthopedic screw (MgYREZr-alloy) in a rabbit model for up to 12 months, J. Biomater. Appl. 28 (2014) 667–675.

[9] T.A. Huehnerschulte, J. Reifenrath, B.v. Rechenberg, D. Dziuba, J. Seitz, D. Bormann, H. Windhagen, A. Meyer-Lindenberg, In vivo assessment of the host reactions to the biodegradation of the two novel magnesium alloys ZEK100 and AX30 in an animal model, Biomed. Eng. Online 11 (2012) 14.

[10] M.P. Sealy, Y.B. Guo, J.F. Liu, C. Li, Pulsed laser cutting of magnesium-calcium for biodegradable stents, Procedia CIRP 42 (2016) 67–72.

[11] E. Charpentier, A. Barna, L. Guillevin, J. Juliard, Fully bioresorbable drug-eluting coronary scaffolds: a review, Arch.Cardiovasc. Dis. 108 (2015) 385–397.

[12] J. Iqbal, Y. Onuma, J. Ormiston, A. Abizaid, R. Waksman, P. Serruys, Bioresorbable scaffolds: rationale, current status, challenges, and future, Eur. Heart J. 35 (2014) 765–776.

[13] C. Di Mario, H. Griffiths, O. Goktekin, N. Peeters, J. Verbist, M. Bosier, K. Deloose, B. Heublein, R. Rohde, V. Kasese, C. Ilsley, R. Erbel, Drug-Eluting bioabsorbable magnesium stent, J. Interv. Cardiol. 17 (2004) 391–395.

[14] P. Peeters, M. Bosiers, J. Verbist, K. Deloose, B. Heublein, Preliminary results after

application of absorbable metal stents in patients with critical limb ischemia, J. Endovasc. Ther. 12 (2005) 1–5.

[15] P. Zartner, R. Cesnjevar, H. Singer, M. Weyand, First successful implantation of a biodegradable metal stent into the left pulmonary artery of a preterm baby, Cathet. Cardiovasc. Interv. 66 (2005) 590–594.

[16] R. Waksman, R. Erbel, C. Di Mario, J. Bartunek, B. de Bruyne, F.R. Eberli, P. Erne, Michael Haude, M. Horrigan, C. Ilsley, D. Böse, H. Bonnier, J. Koolen, T.F. Lüscher, N.J. Weissman, Early- and long-term intravascular ultrasound and angiographic findings after bioabsorbable magnesium stent implantation in human coronary arteries, JACC, Cardiovascular Interventions 2 (2009) 312–320.

[17] H. Hermawan, D. Dubé, D. Mantovani, Degradable metallic biomaterials: design and development of Fe-Mn alloys for stents, J. Biomed. Mater. Res. (2010) 1–11 Part A 93A.

[18] S.A. Luffy, D. Chou, J. Waterman, P.D. Wearden, P.N. Kumta, T.W. Gilbert, Evaluation of magnesium-yttrium alloy as an extraluminal tracheal stent, J. Biomed. Mater. Res. A 102 (2014) 611–620.

[19] Y. Jang, D. Owuor, J.T. Waterman, L. White, C. Boyce, J. Sankar, T.W. Gilbert, Y. Yun, Effect of mucin and bicarbonate ion on corrosion behavior of AZ31 magnesium alloy for airway stents, Materials 7 (2014) 5866–5882.

[20] S. Zhang, Y. Zheng, L. Zhang, Y. Bi, J. Li, J. Liu, H. Guo, Y. Li, In vitro and in vivo corrosion and histocompatibility of pure Mg and a Mg-6Zn alloy as urinary implants in rat model, Mater. Sci. Eng. C 68 (2016) 414–422.

[21] J. Seitz, A. Lucas, M. Kirschner, Magnesium-based compression screws: a novelty in the clinical use of implants, JOM 68 (2016) 1177–1182.

[22] U&i Corporation, History, http://www.youic.com/m/sub01/02.php, (2019).

[23] M. Schildwächter, S.E. Biotronik, K.G. Co, Switzerland Buelach, Biotronik Press Release Biotronik Announces CE Mark for Magmaris, the First Clinically-Proven Bioresorbable Magnesium Scaffold, (2016).

[24] H. Hornberger, S. Virtanen, A.R. Boccaccini, Biomedical coatings on magnesium alloys – a review, Acta Biomater. 8 (2012) 2442–2455.

[25] Z. Chun-Yan, Z. Rong-Chang, L. Cheng-Long, G. Jia-Cheng, Comparison of calcium phosphate coatings on Mg–Al and Mg–Ca alloys and their corrosion behavior in Hank's solution, Surf. Coat. Technol. 204 (2010) 3636–3640.

[26] J. Waterman, M.P. Staiger, Coating systems for magnesium-based biomaterials - state of the art, Magnes.Technol. 2011 (2011) 403–408.

[27] N.T. Kirkland, N. Birbilis, Magnesium Biomaterials : Design, Testing, and Best Practice, Springer, Cham, 2013.

[28] G.L. Song, A. Atrens, Corrosion mechanisms of magnesium alloys, Adv. Eng. Mater. 1 (1999) 11–33.

[29] A.C. Hänzi, P. Gunde, M. Schinhammer, P.J. Uggowitzer, On the biodegradation performance of an Mg–Y–RE alloy with various surface conditions in simulated body fluid, Acta Biomater. 5 (2009) 162–171.

[30] LSP Technologies, Surface distribution of residual stresses, http://www.lsptechnologies.com/cs-effects-on-surface-residual-stress.php, (2014).

[31] Y. Guo, M.P. Sealy, C. Guo, Significant improvement of corrosion resistance of biodegradable metallic implants processed by laser shock peening, CIRP Ann. - Manuf. Technol. 61 (2012) 583–586.

[32] M.P. Sealy, Y.B. Guo, Surface integrity and process mechanics of laser shock peening of novel biodegradable magnesium–calcium (Mg–Ca) alloy, J. Mech. Behav. Biomed. Mater. 3 (2010) 488–496.

[33] M.P. Sealy, Y.B. Guo, R.C. Caslaru, J. Sharkins, D. Feldman, Fatigue performance of biodegradable magnesium–calcium alloy processed by laser shock peening for orthopedic implants, Int. J. Fatigue 82 (2016) 428–436.

[34] M. Salahshoor, Y.B. Guo, Biodegradation control of magnesium-calcium biomaterial via adjusting surface integrity by synergistic cutting-burnishing, Procedia CIRP 13 (2014) 143–149.

[35] M.P. Sealy, Y.B. Guo, Fabrication and Characterization of Surface Texture for Bone Ingrowth by Sequential Laser Peening Biodegradable Orthopedic Magnesium-Calcium Implants vol. 5, (2011), p. 9.

[36] M.P. Sealy, Z. Liu, C. Li, Y. Guo, B. White, M. Barkey, B. Jordon J, L.N. Brewer, D. Feldman, A strategy to optimize recovery in orthopedic sports injuries, J. Bioanal. Biomed. 9 (2017).

[37] M. Gieseke, C. Noelke, S. Kaierle, V. Wesling, H. Haferkamp, Selective laser melting of magnesium and magnesium alloys, Magnesium Technology, John Wiley & Sons, Inc, Hoboken, NJ, USA, 2013, pp. 65–68 2013.

[38] X. Niu, H. Shen, J. Fu, Microstructure and mechanical properties of selective laser melted Mg-9 wt%Al powder mixture, Mater. Lett. 221 (2018) 4–7.

[39] K. Wei, Z. Wang, X. Zeng, Influence of element vaporization on formability, composition, microstructure, and mechanical performance of the selective laser melted Mg–Zn–Zr components, Mater. Lett. 156 (2015) 187–190.

[40] A. Pawlak, M. Rosienkiewicz, E. Chlebus, Design of experiments approach in AZ31 powder selective laser melting process optimization, Arch. Civ. Mech. Eng. 17 (2017) 9–18.

[41] C.C. Ng, M.M. Savalani, M.L. Lau, H.C. Man, Microstructure and mechanical properties of selective laser melted magnesium, Appl. Surf. Sci. 257 (2011) 7447–7454.

[42] M.M. Savalani, J.M. Pizarro, Effect of preheat and layer thickness on selective laser melting (SLM) of magnesium, Rapid Prototyp. J. 22 (2016) 115–122.

[43] C. Chung Ng, M. Savalani, H. Chung Man, Fabrication of magnesium using selective laser melting technique, Rapid Prototyp. J. 17 (2011) 479–490.

[44] Y. Guo, H. Pan, L. Ren, G. Quan, Microstructure and mechanical properties of wire arc additively manufactured AZ80M magnesium alloy, Mater. Lett. 247 (2019) 4–6.

[45] J. Guo, Y. Zhou, C. Liu, Q. Wu, X. Chen, J. Lu, wire arc additive manufacturing of AZ31 magnesium alloy: grain refinement by adjusting pulse frequency, Materials 9 (2016) 823.

[46] M.M. Farag, H. Yun, Effect of gelatin addition on fabrication of magnesium phosphate-based scaffolds prepared by additive manufacturing system, Mater. Lett. 132 (2014) 111–115.

[47] S. Palanivel, P. Nelaturu, B. Glass, R.S. Mishra, Friction stir additive manufacturing

[48] M. Salehi, S. Maleksaeedi, S.M.L. Nai, G.K. Meenashisundaram, M.H. Goh, M. Gupta, A paradigm shift towards compositionally zero-sum binderless 3D printing of magnesium alloys via capillary-mediated bridging, Acta Mater. 165 (2019) 294–306.

[49] M. Salehi, S. Maleksaeedi, M.A.B. Sapari, M.L.S. Nai, G.K. Meenashisundaram, M. Gupta, Additive manufacturing of magnesium–zinc–zirconium (ZK) alloys via capillary-mediated binderless three-dimensional printing, Mater. Des. 169 (2019) 107683.

[50] Y. Li, J. Zhou, P. Pavanram, M.A. Leeflang, L.I. Fockaert, B. Pouran, N. Tümer, K.-. Schröder, J.M.C. Mol, H. Weinans, H. Jahr, A.A. Zadpoor, Additively manufactured biodegradable porous magnesium, Acta Biomater. 67 (2018) 378–392.

[51] F. Witte, V. Kaese, H. Haferkamp, E. Switzer, A. Meyer-Lindenberg, C.J. Wirth, H. Windhagen, In vivo corrosion of four magnesium alloys and the associated bone response, Biomaterials 26 (2005) 3557–3563.

[52] ASTM International, Standard Terminology for Additive Manufacturing, (2015).

[53] J. Kruth, P. Mercelis, J. Van Vaerenbergh, L. Froyen, M. Rombouts, Binding mechanisms in selective laser sintering and selective laser melting, Rapid Prototyp. J. 11 (2005) 26–36.

[54] F. Bär, L. Berger, L. Jauer, G. Kurtuldu, R. Schäublin, J.H. Schleifenbaum, J.F. Löffler, Laser additive manufacturing of biodegradable magnesium alloy WE43: a detailed microstructure analysis, Acta Biomater. 98 (2019) 36–49.

[55] C.C. Ng, M.M. Savalani, H.C. Man, I. Gibson, Layer manufacturing of magnesium and its alloy structures for future applications, Virtual Phys. Prototyp. 5 (2010) 13–19.

[56] X. Niu, H. Shen, J. Fu, J. Yan, Y. Wang, Corrosion behaviour of laser powder bed fused bulk pure magnesium in hank's solution, Corros. Sci. 157 (2019) 284–294.

[57] S. Gangireddy, B. Gwalani, K. Liu, E.J. Faierson, R.S. Mishra, Microstructure and mechanical behavior of an additive manufactured (AM) WE43-Mg alloy, Addit. Manuf. 26 (2019) 53–64.

[58] W. Li, Y. Li, H. Jahr, X. Zhang, M.A. Leeflang, B. Pouran, F.D. Tichelaar, H. Weinans, J. Zhou, A.A. Zadpoor, Biodegradation-affected fatigue behavior of additively manufactured porous magnesium, Addit. Manuf. 28 (2019) 299–311.

[59] B. Zhang, H. Liao, C. Coddet, Effects of processing parameters on properties of selective laser melting Mg–9%Al powder mixture, Mater. Des. 34 (2012) 753–758.

[60] S. Liu, W. Yang, X. Shi, B. Li, S. Duan, H. Guo, J. Guo, Influence of laser process parameters on the densification, microstructure, and mechanical properties of a selective laser melted AZ61 magnesium alloy, J. Alloy. Comp. 808 (2019) 1–16 151160.

[61] K. Wei, M. Gao, Z. Wang, X. Zeng, Effect of energy input on formability, microstructure and mechanical properties of selective laser melted AZ91D magnesium alloy, Mater. Sci. Eng. A 611 (2014) 212–222.

[62] D. Schmid, J. Renza, M.F. Zaeh, J. Glasschroeder, Process influences on laser-beam melting of the magnesium alloy AZ91, Physics Procedia 83 (2016) 927–936.

[63] Y. Yin, Q. Huang, L. Liang, X. Hu, T. Liu, Y. Weng, T. Long, Y. Liu, Q. Li, S. Zhou, H. Wu, In vitro degradation behavior and cytocompatibility of ZK30/bioactive glass composites fabricated by selective laser melting for biomedical applications, J. Alloy. Comp. 785 (2019) 38–45.

[64] C. Liu, M. Zhang, C. Chen, Effect of laser processing parameters on porosity, microstructure and mechanical properties of porous Mg-Ca alloys produced by laser additive manufacturing, Mater. Sci. Eng. A 703 (2017) 359–371.

[65] D. Hu, Y. Wang, D. Zhang, L. Hao, J. Jiang, Z. Li, Y. Chen, Experimental investigation on selective laser melting of bulk net-shape pure magnesium, Mater. Manuf. Process. 30 (2015) 1298–1304.

[66] K. Wei, X. Zeng, Z. Wang, J. Deng, M. Liu, G. Huang, X. Yuan, Selective laser melting of Mg-Zn binary alloys: effects of Zn content on densification behavior, microstructure, and mechanical property, Mater. Sci. Eng. A 756 (2019) 226–236.

[67] M. Salehi, S. Maleksaeedi, H. Farnoush, M.L.S. Nai, G.K. Meenashisundaram, M. Gupta, An investigation into interaction between magnesium powder and Ar gas: implications for selective laser melting of magnesium, Powder Technol. 333 (2018) 252–261.

[68] H. Takagi, H. Sasahara, T. Abe, H. Sannomiya, S. Nishiyama, S. Ohta, K. Nakamura, Material-property evaluation of magnesium alloys fabricated using wire-and-arc-based additive manufacturing, Addit. Manuf. 24 (2018) 498–507.

[69] E. Vorndran, C. Moseke, U. Gbureck, 3D printing of ceramic implants, MRS Bull. 40 (2015) 127–136.

[70] S. Meininger, C. Moseke, K. Spatz, E. März, C. Blum, A. Ewald, E. Vorndran, Effect of strontium substitution on the material properties and osteogenic potential of 3D powder printed magnesium phosphate scaffolds, Mater. Sci. Eng. C 98 (2019) 1145–1158.

[71] S. Meininger, S. Mandal, A. Kumar, J. Groll, B. Basu, U. Gbureck, Strength reliability and in vitro degradation of three-dimensional powder printed strontium-substituted magnesium phosphate scaffolds, Acta Biomater. 31 (2016) 401–411.

[72] L. Li, J. Gao, Y. Wang, Evaluation of cyto-toxicity and corrosion behavior of alkali-heat-treated magnesium in simulated body fluid, Surf. Coat. Technol. 185 (2004) 92–98.

[73] G. Song, S. Song, A possible biodegradable magnesium implant Material, Adv. Eng. Mater. 9 (2007) 298–302.

[74] F. Witte, The history of biodegradable magnesium implants: a review, Acta Biomater. 6 (2010) 1680–1692.

[75] C. Shuai, L. Liu, M. Zhao, P. Feng, Y. Yang, W. Guo, C. Gao, F. Yuan, Microstructure, biodegradation, antibacterial and mechanical properties of ZK60-Cu alloys prepared by selective laser melting technique, J. Mater. Sci. Technol. 34 (2018) 1944–1952.

[76] R. Xu, M. Zhao, Y. Zhao, L. Liu, C. Liu, C. Gao, C. Shuai, A. Atrens, Improved biodegradation resistance by grain refinement of novel antibacterial ZK30-Cu alloys produced via selective laser melting, Mater. Lett. 237 (2019) 253–257.